Kilometer-scale sound speed structure that affects GNSS-A observation: Case study off the Kii channel

Yusuke Yokota[1*], Tadashi Ishikawa[2], Shun-ichi Watanabe[2], Yuto Nakamura[2]

[1]Institute of Industrial Science, University of Tokyo, 4-6-1, Komaba, Meguro-ku, Tokyo, Japan

[2]Hydrographic and Oceanographic Department, Japan Coast Guard, 3-1-1, Kasumigaseki, Chiyoda-ku, Tokyo, Japan

*** Correspondence:**
Yusuke Yokota
yyokota@iis.u-tokyo.ac.jp

Keywords: GNSS-A, GNSS-A oceanography, sound speed structure, Kuroshio, Kii channel

Abstract

The Global Navigation Satellite System-Acoustic ranging combination technique (GNSS-A) is a recently developed technology to precisely detect seafloor crustal deformation. This method can also estimate km-scale underwater sound speed structure (SSS) as a by-product of monitoring seafloor crustal deformation. This paper evaluates the validity of the spatial gradient and its temporal variation of the SSS estimated by GNSS-A observations off the Kii channel before and after Kuroshio meandering. According to the comparison of the JCOPE2M reanalysis data and the in-situ observation data, the GNSS-A estimated SSS has local structures that are not reproduced in the reanalysis. In addition, we investigate the effect of observation time on the stability of SSS estimation. The results suggest that the sufficient time required for stable estimation depends on the spatial coverage of observation data, which depends on the depth of the site. As a result, the time resolution was derived to be about one hour at a site whose depth is 1500 m.

1 Introduction

The Global Navigation Satellite System-Acoustic ranging combination technique (GNSS-A) was proposed and developed to extend the geodetic network to the seafloor by combining GNSS positioning with acoustic ranging technology (Spiess, 1985; Asada and Yabuki, 2001; Fujita et al., 2006). This observation technique makes it possible to accurately measure the seafloor movement and to detect various subseafloor geophysical phenomena due to co-, post-, and inter-seismic phases following a huge earthquake cycle (e.g., Sato et al., 2011; Watanabe et al., 2014; Yokota et al., 2016). Recently, Yokota and Ishikawa (2020) reported detection of tiny transient signals due to slow slip events. To monitor this kind of transient signals continuously, it is indispensable to upgrade the GNSS-A accuracy, which requires a better understanding of the underwater sound speed structure (SSS).

The uncertainty of the SSS is a major error source of GNSS-A observation. Our group has been developing analysis methods to estimate the SSS from GNSS-A observation (Fujita et al., 2006; Yokota et al., 2019). For example, Yokota and Ishikawa (2019) confirmed that the GNSS-A estimated SSS off the Bungo channel is almost consistent with the temperature gradient structure caused by the Kuroshio.

This paper conducts surveys on the spatial gradient of SSS that affects the GNSS-A, by comparison between its analysis results and the ocean structure off the Kii channel before and after Kuroshio meandering. The estimated parameters are compared with ocean reanalysis data and in-situ expendable bathythermographs (XBTs) and expendable conductivity temperature depth (XCTD) profilers data. The results depend on whether the Kuroshio is meandering or not. Especially in the case when the Kuroshio meandered, GNSS-A estimated SSS has a gradient that was not reproduced in the reanalysis. Additionally, we examine the temporal variation of the gradient parameters.

2 Gradient parameters extracted from GNSS-A oceanography

2.1 Method

In the GNSS-A, to measure the movement of the seafloor accurately, the absolute position of a relay point located on the sea surface is determined by the GNSS, and the relative position between the relay point and the seafloor station is determined by acoustic ranging. As a result, the absolute seafloor position can be determined. The observation system is shown in Fig. 1a. Please see Yokota et al. (2018) for details.

In the present day, the horizontal positioning accuracy of the GNSS-A is about 2 cm (1σ). Because the spatiotemporal variations of the SSS are more complex and larger than those of the ionosphere/troposphere which affect the GNSS positioning, the uncertainty of SSS is the largest error source of GNSS-A. Data obtained from in-situ observations such as XBT/XCTD measurements can constrain the SSS, but cannot cover all of these variations in detail. Therefore, developing an analysis method for estimating the SSS in detail is an important research target for GNSS-A observation.

After the early work of Fujita et al. (2006) which estimates the temporal variation of the SSS by quadratic polynomial approximation, various techniques to process underwater SSS have been studied. Yokota et al. (2019) reinterpreted Fujita's method and developed a technique that determines the shallow horizontal gradient of the SSS by performing pseudo-tomographic analysis within the triangle V_1 (Fig. 1b) connecting the moving ship and the seafloor station. Additionally, estimation of the SSS when fluctuations occur in deeper regions has been improved by using another triangle V_2 (Fig. 1b). Their detailed methodologies are described in Yokota et al. (2019), Yokota and Ishikawa (2019), and Yokota (2019).

Generally, to understand the ocean structure, satellite observations are used to capture the global ocean surface property and in-situ observations, such as XBT/XCTD, Argo float, are used to capture the vertical profile at a local point. In the GNSS-A, the overview of the horizontal gradient of the SSS is obtained. Because the spatial range of the obtained gradient depends on the size of the transponder deployment region, which is typically in the range of 2-6 km, the GNSS-A estimated SSS can have a slightly different perspective than those of other ocean observations. The GNSS-A may reveal structures that cannot be detected by other observations. Although there is no other way to precisely measure SSS in km-scale than costly XBT/XCTD dense observations, we examine the appropriateness of the GNSS-A estimation results by comparing with other data having different spatial scales such as in-situ and reanalysis data.

2.2 Data

Here, we use the data obtained at two sites off the Kii channel, namely, MRT1 and MRT2 in June 2013 (1306), April 2018 (1804), July 2018 (1807), and November 2018 (1811). The gradient parameters estimated from GNSS-A data for each observation campaign are represented as vectors V_1 and V_2 as shown in Fig. 2. Although the vectors can be obtained for each acoustic shot data continuously, in sections 3 and 4, we discuss using the time average value from all acoustic shot data. Temporal variation of gradient vectors will be discussed in section 5.

The vector is pointing in the direction of higher sound speed. In 1306 and 1811, V_1 is sufficiently larger than V_2. This suggests that the SSS has a gradient only in the relatively shallow layers, from the considerations in Yokota (2019). However, the thickness of the gradient layer cannot be uniquely estimated. In contrast, the result obtained at site MRT2 in 1804 shows that V_2 is larger than V_1. This suggests that a gradient has emerged in a relatively deeper region. Small vectors at site MRT1 in 1807 suggest a weak gradient SSS.

3 Comparison with JCOPE2M reanalysis data

JCOPE2M is an ocean reanalysis data targeting the northwestern Pacific Ocean, produced by assimilating satellite and in-situ observation data to an ocean model using a multi-scale three-dimensional variational scheme (Miyazawa et al., 2017; Miyazawa et al., 2019). The model is based on the Princeton Ocean Model, with a horizontal resolution of 1/12 degrees. The model can express 10-100 km scale oceanographic phenomena, but detailed structure on the km-scale has not been completely represented. Here, we compare the GNSS-A estimated gradient vector of SSS with the JCOPE2M reanalysis.

Fig. 2 shows the temperature and its gradient at 100 m depth, derived from the reanalysis during each observation campaign. In 1306, the northern edge of the Kuroshio lies around the vicinity of MRT1 and MRT2. The large southward gradient field V_1 is consistent with the reanalysis (Fig. 2a). This result is similar as ones off the Bungo channel (Yokota and Ishikawa, 2019), when the Kuroshio flows near the GNSS-A site.

After August 2017, when the Kuroshio began to meander, the southward gradient vectors around the two sites changed because warm seawater advected to the south (Figs 2b-d). In 1807 (Fig. 2c), site MRT1 was located far from Kuroshio, and site MRT2 was located at the edge region of Kuroshio. Small extracted vectors at site MRT1 and southward vectors at site MRT2 are consistent with the reanalysis.

In 1804 (Fig. 2b), the reanalysis indicates very weak gradients around the sites, because the Kuroshio was far away from the sites. In contrast, GNSS-A estimates a northward gradient vector which is inconsistent with reanalysis. In 1811 (Fig. 2d), northward vectors at MRT2 were also inconsistent with a slight southward gradient in the reanalysis.

4 Comparison with in-situ sound speed observation

To clarify the inconsistency between the GNSS-A estimation and the reanalysis, in-situ observation was carried out along a line crossing the Kuroshio in 1811. XBT/XCTD were dropped sequentially at evenly spaced points as shown in Fig. 3a. Fig. 3b shows the cross section of the underwater SSS, generated from the XBT and XCTD data.

This result shows that there is a northward gradient around 33.2N-33.5N and a southward gradient around 32.7N-32.8N which are consistent with the reanalysis. In addition, there are partially complicated structures that do not appear in the reanalysis around 32.8N-32.9N and 33.1N. The northward GNSS-A result at site MRT2, which is inconsistent with the reanalysis, may reflect the km-scale structure shown in this in-situ observation. This result suggests that GNSS-A was influenced by a detailed SSS that was not resolved in the reanalysis.

However, without costly dense (spatial and temporal) in-situ observation, it is difficult to verify the GNSS-A extraction results in such a complicated case. To apply the GNSS-A estimated SSS oceanographically and to enhance the GNSS-A observation accuracy, more oceanographic in-situ observations and validations will be necessary.

The km-scale structure may reflect the complexity of the underwater structure, such as internal gravity waves. In the vicinity of our study area, the Tosa-bae bump (see Fig. 3) may have triggered such a complicated SSS. Matsui et al. (2019) showed that internal gravity waves driven by such topographic peaks affect GNSS-A positioning accuracy, using numerical simulation.

5 Temporal resolution

Up to the above section, we discussed using gradient values that have been time averaged over the entire observation time in each observation campaign. In principle, the gradient vector is estimated for each acoustic shot, which makes it possible to detect the time variation of the gradient vector. Yokota et al. (2019) and Yokota and Ishikawa (2019) visualized the time variation of the gradient vectors using one round of the survey line as shown in Fig. 4a. However, the estimation of the gradient vector is stable only when the survey lines cover the whole observation area. Figs 4b-d show the effect of data coverage on the estimation of gradient vector in the cases using half, one third, and a quarter of all survey lines.

Fig. 4 shows that the gradient vectors become unstable as the coverage of the observation area becomes narrower. As shown in the layout of the survey lines, the estimation sensitivity is weak when the survey lines are perpendicular to the gradient, because the data coverage area in the direction of the gradient becomes narrower. In most cases, the SSS around site MRT2 has a meridional gradient since the flow of Kuroshio off the Kii channel is mainly eastward. Therefore, when the survey line covers only in the zonal direction (for example, in Fig. 4d, second vector), a correct gradient cannot be detected.

From the above discussion, the time resolution of the GNSS-A estimated gradient vector for site MRT2 is about one hour at best, which is enough time to evenly cover the observation area. However, as with the case of spatial resolution, there is almost no model or in-situ observation that can explain the hourly order fluctuations, making it difficult to verify whether the temporal variation of the estimated gradient vector reflects the actual underwater structure.

As shown in Fig. 1b, the survey line length is set to be broadened depending on the depth so that the triangle size is large enough for stable estimation. Practically, the diagonal length of the survey lines is set to be approximately twice the depth of the site. Therefore, the observation time required to evenly cover all directions depends on the depth of the site. In the case of MRT2, whose depth is 1500 m, the time resolution is about one hour. Thus, the time resolution T at a site with an arbitrary depth is estimated as follows:

$$T \sim 1 * \text{depth (m)} / 1500 \text{ (m) [hour]} \qquad (1)$$

The time resolution derived from this relationship is about 2 hours for a 3000 m depth site, and about 40 minutes for a 1000 m depth site. However, this is just a provisional result that needs to be confirmed by further research.

6 Future Works

It is considered that the gradient SSSs off the Kii channel shown here reflects not only the large structures due to the Kuroshio but also small scale fluctuations that are not easy to obtain appropriate data for comparison. In the future, further confirmation of the estimated gradient parameters will contribute not only to improve the accuracy of GNSS-A observations but also to assist the exploration of km-scale ocean fields that cannot be easily observed with the existing oceanographic methods.

7 Conflict of Interest

The authors declare that they have no conflict of interest.

8 Data Availability

The GNSS-A data needed to evaluate the conclusions are present in the paper. The XBT/XCTD underwater sound speed data is available in the PANGAEA website (Seafloor Geodesy Group, 2020). The JCOPE2M data is available in the JCOPE2M website (http://www.jamstec.go.jp/jcope/htdocs/e/home.html).

9 Author Contributions

YY designed the study and wrote this manuscript. YY and TI have led the direct observation of SSS. YY, TI, SW, and YN discussed about the analysis method and commented to improving the manuscript.

10 Funding

The submission of this manuscript was funded by the University of Tokyo.

11 Acknowledgments

We would like to thank the Geospatial Information Authority of Japan (GSI) for providing high-rate GNSS data for the kinematic GNSS analysis and daily coordinates of the GEONET sites (Sagiya et al., 2000; Nakagawa et al., 2009) on the GSI website. Many members of the staff of the Hydrographic and Oceanographic Department, Japan Coast Guard, including the crew of the survey vessels Takuyo, Shoyo, Meiyo, and Kaiyo, supported our observations and technological developments. We also thank for devoted maintenance and management by active and senior staffs in the Geodesy and Geophysics Office, Hydrographic and Oceanographic Department of Japan Coast Guard.

References

Asada, A., and Yabuki, T. (2001). Centimeter-level positioning on the seafloor. Proc. Jpn Acad. Ser. B 77, 7-12.

Fujita, M., Ishikawa, T., Mochizuki, M., Sato, M., Toyama, S., Katayama, M., Kawai, K., Matsumoto, Y., Yabuki, T., Asada, A., Colombo, O. L. (2006). GPS/acoustic seafloor geodetic observation:

method of data analysis and its application. Earth Planet. Space 58, 265-275. doi:10.1007/s00190-013-0649-9

Matsui, T., Kido, M., Niwa, Y., Honsho, C. (2019). Effects of disturbance of seawater excited by internal wave on GNSS-acoustic positioning. Mar. Geophys. Res. doi:10.1007/s11001-019-09394-6

Miyazawa, Y., Varlamov, S. M., Miyama, T., Guo X, T., Hihara, T., Kiyomatsu, K., Kachi, M., Kurihara, Y., Murakami, H. (2017). Assimilation of high-resolution sea surface temperature data into an operational nowcast/forecast system around Japan using a multi-scale three dimensional variational scheme. Ocean Dynamics 67, 713-728. doi:10.1007/s10236-017-1056-1

Miyazawa, Y., Kuwano-Yoshida, A., Doi, T., Nishikawa, T., Narazaki, T., Fukuoka, T., Sato, K. (2019). Temperature profiling measurements by sea turtles improve ocean state estimation in the Kuroshio-Oyashio Confluence region. Ocean Dynamics 69, 267-282. doi:10.1007/s10236-018-1238-5

Nakagawa, H., et al. (2009). Development and validation of GEONET new analysis strategy (Version 4), J. Geograph. Surv. Inst., 118, 1-8.

Sagiya, T., Miyazaki, S., and Tada, T. (2000). Continuous GPS array and present-day crustal deformation of Japan. Pure Appl. Geophys. 157, 2303-2322. doi:10.1007/PL00022507

Sato, M., Ishikawa, T., Ujihara, N., Yoshida, S., Fujita, M., Mochizuki, M., and Asada, A. (2011). Displacement above the hypocenter of the 2011 Tohoku-oki earthquake. Science 332:1395. doi:10.1126/science.1207401

Seafloor Geodesy Group (2020). Cross-section underwater sound speed observation data off the Kii Channel on November 23, 2018. PANGAEA doi:10.1594/PANGAEA.915138

Spiess, F. N. (1985). Suboceanic geodetic measurements. IEEE Trans. Geosci. Remote Sensing GE-23, 502-510.

Watanabe, S., Sato, M., Fujita, M., Ishikawa, T., Yokota, Y., Ujihara, N., and Asada, A. (2014). Evidence of viscoelastic deformation following the 2011 Tohoku-oki earthquake revealed from seafloor geodetic observation. Geophys. Res. Lett. 41:5789-5796. doi:10.1002/2014GL061134

Yokota, Y., Ishikawa, T., Watanabe, S., Tashiro, T., and Asada, A. (2016). Seafloor geodetic constraints on interplate coupling of the Nankai Trough megathrust zone. Nature 534:374-377. doi:10.1038/nature17632

Yokota, Y., Ishikawa, T., Watanabe, S. (2018). Seafloor crustal deformation data along the subduction zones around Japan obtained by GNSS-A observations. Scientific Data 5, 180182. doi:10.1038/sdata.2018.182

Yokota, Y. (2019). Quantitative interpretation of the ability of the GNSS-A to monitor underwater structure. Journal of Marine Acoustic Society of Japan 46, 3, 116-129.

Yokota, Y., Ishikawa, T. (2019). Gradient field of undersea sound speed structure extracted from the GNSS-A oceanography: GNSS-A as a sensor for detecting sound speed gradient. SN Applied

Sciences 1, 693. doi:10.1007/s42452-019-0699-6

Yokota, Y., Ishikawa, T., Watanabe, S. (2019). Gradient field of undersea sound speed structure extracted from the GNSS-A oceanography. Mar. Geophys. Res. 40, 4, 493-504. doi:10.1007/s11001-018-9362-7

Yokota, Y., Ishikawa, T. (2020). Shallow slow slip events along the Nankai Trough detected by GNSS-A. Science Advances 6, eaay5786. doi:10.1126/sciadv.aay5786

Figure legends

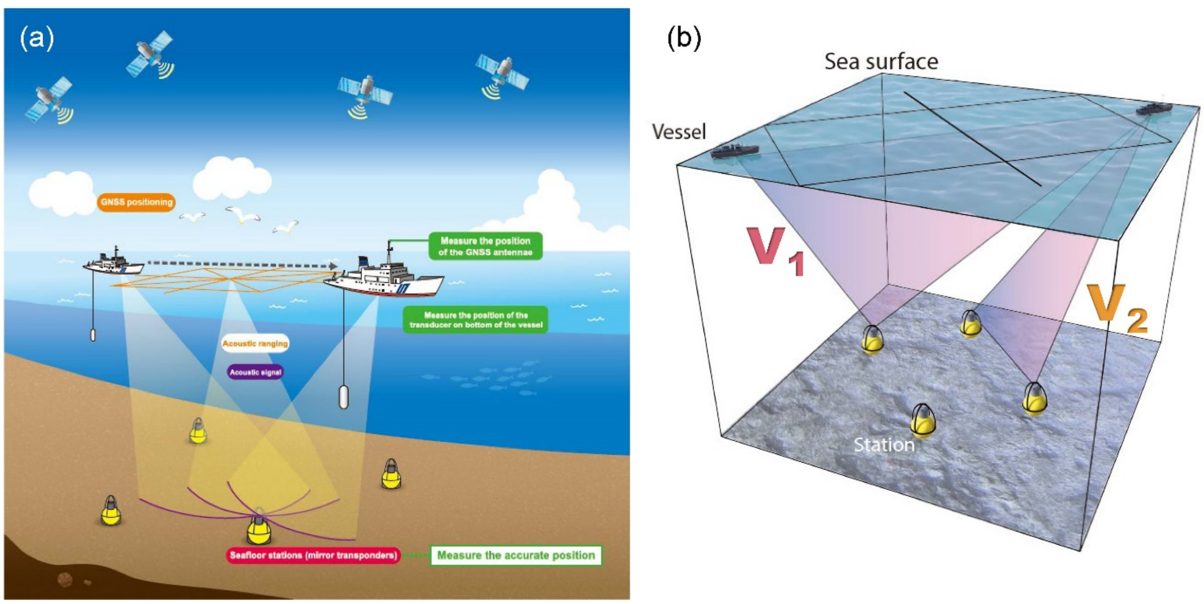

Figure 1. (a) A schematic image of the GNSS-A system. (b) A schematic image of scanning SSS. These figures are modified after Yokota et al. (2018, 2019).

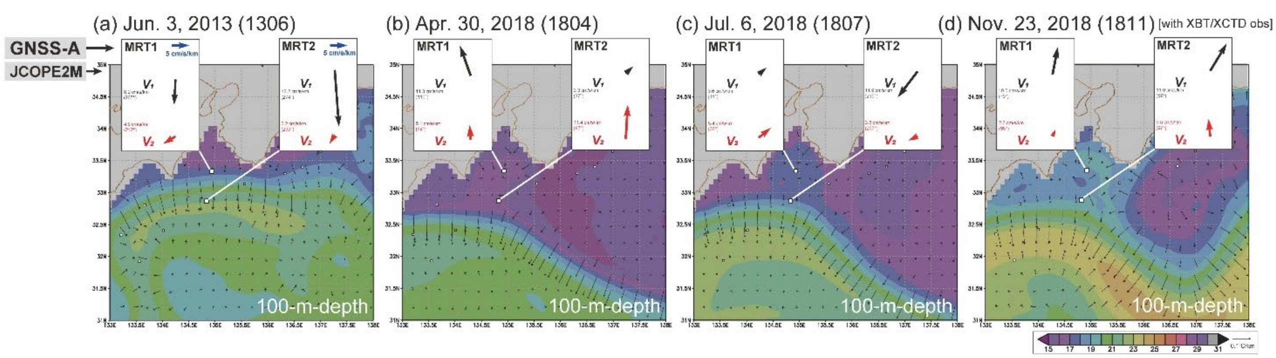

Figure 2. Gradient parameters extracted in GNSS-A (black (V_1) and red (V_2) vectors) and 100 m-depth temperature fields of the JCOPE2M reanalysis on observation dates, (a) Jun. 3, 2013, (b) Apr. 30, 2018, (c) Jul. 6, 2018, and (d) Nov. 23, 2018 for MRT1 and MRT2. The value of each vector (absolute value and counterclockwise angle from east) is written beside the vector. Scales of the

water temperature and the temperature gradient vector of the JCOPE2M reanalysis are shown on the bottom right.

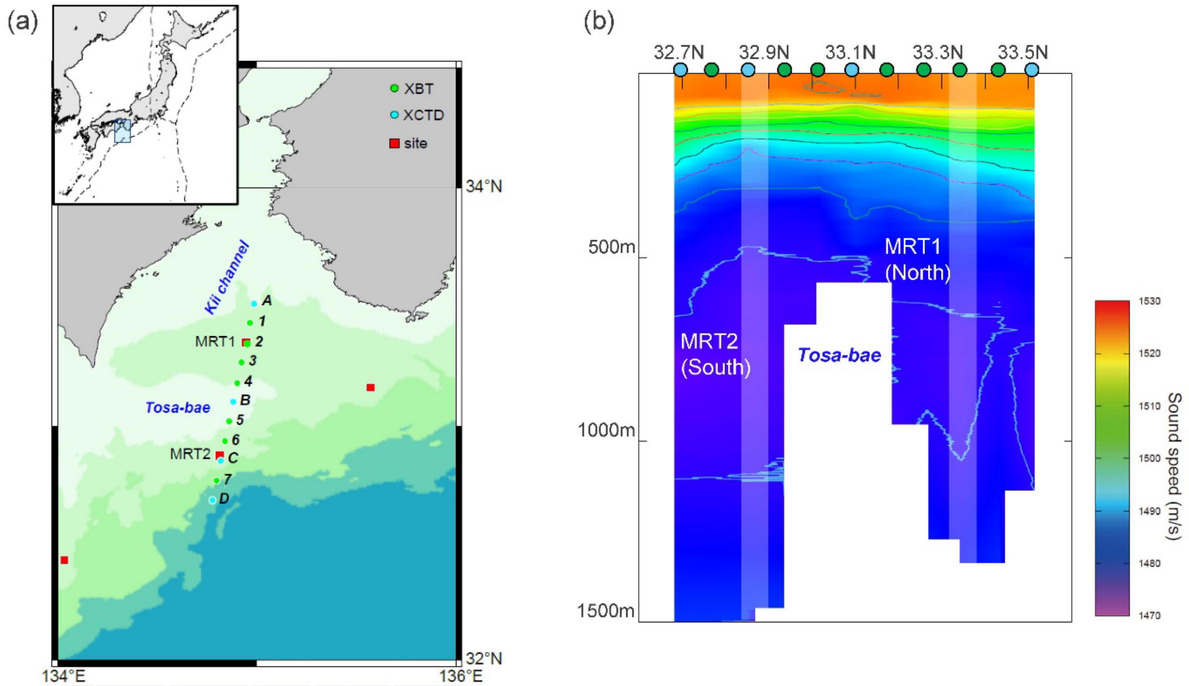

A	33.5131N	134.9858E	Nov. 23	ETC12:51	XCTD
1	33.4332N	134.9653E	Nov. 23	ETC13:19	XBT
2	33.3450N	134.9517E	Nov. 23	ETC11:34	XBT
3	33.2662N	134.9233E	Nov. 23	ETC14:18	XBT
4	33.1789N	134.9013E	Nov. 23	ETC14:51	XBT
B	33.0996N	134.8812E	Nov. 23	ETC15:22	XCTD
5	33.0168N	134.8604E	Nov. 23	ETC15:48	XBT
6	32.9334N	134.8393E	Nov. 23	ETC16:16	XBT
C	32.8500N	134.8185E	Nov. 23	ETC16:44	XCTD
7	32.7656N	134.7973E	Nov. 23	ETC17:22	XBT
D	32.6824N	134.7766E	Nov. 23	ETC17:43	XCTD

Figure 3. (a) Locations of the seafloor sites and direct sound speed observation points in November 2018. Red squares indicate seafloor sites MRT1 and MRT2. Green and light-blue circles indicate XBT and XCTD observation points, respectively. Details of XBT and XCTD casts are listed in the bottom table. (b) Resultant SSS cross section of direct observations. White bars indicate regions around sites MRT1 and MRT2. Green and blue circles at the surface indicate positions of the XBT and XCTD casts, respectively.

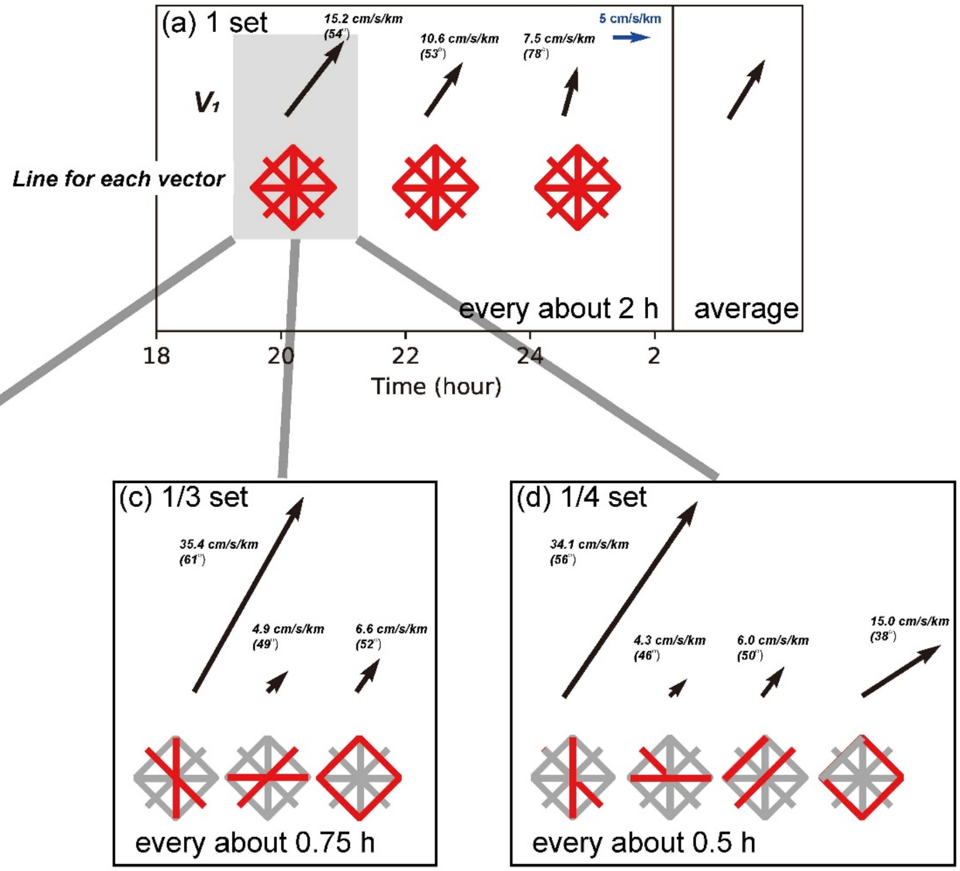

Figure 4. Time series of the gradient parameters of site MRT2 on Nov. 23, 2018. The cases calculated for one set of survey lines (a; every about 2-hour), divided into two parts (b; every about 1-hour), divided into three parts (c; every about 0.75-hour), and divided into four parts (d; every about 0.5-hour), respectively. Each survey line (red line) shows the approximate line set for calculating each vector. The value of each vector (absolute value and counterclockwise angle from east) is written beside the vector.